RAPID COMMUNICATION

Mixed spin states for strain-robust ferromagnetism in $SrCoO_3$ thin films

Xiquan Zheng(郑希诠)[1], Nicholas B. Brookes[2], Flora Yakhou-Harris[2], Yingjie Lyu(吕英杰)[3], Jianbing Zhang(张建兵)[3], Qian Xiao(肖铅)[1], Xinyi Jiang(蒋心怡)[1], Qingzheng Qiu(仇清正)[1], Qizhi Li(李齐治)[1], Shilong Zhang(张世龙)[1], Xinqiang Cai(蔡新强)[1], Pu Yu(于浦)[3,4], Yi Lu(卢毅)[5,6,†], and Yingying Peng(彭莹莹)[1,7,‡]

[1] *International Center for Quantum Materials, School of Physics, Peking University, Beijing* 100871, *China*
[2] *ESRF-The European Synchrotron*, 71 *Avenue des Martyrs, CS* 40220, *F*-38043 *Grenoble, France*
[3] *State Key Laboratory of Low Dimensional Quantum Physics, Department of Physics, Tsinghua University, Beijing* 100084, *China*
[4] *Frontier Science Center for Quantum Information, Beijing* 100084, *China*
[5] *National Laboratory of Solid State Microstructures and Department of Physics, Nanjing University, Nanjing* 210093, *China*
[6] *Collaborative Innovation Center of Advanced Microstructures, Nanjing University, Nanjing* 210093, *China*
[7] *Collaborative Innovation Center of Quantum Matter, Beijing* 100871, *China*

(Received 15 May 2026; revised manuscript received 29 June 2026; accepted manuscript online 9 July 2026)

Epitaxial strain in transition-metal oxides can induce dramatic changes in electronic and magnetic properties. A recent study on epitaxially strained $SrCoO_3$ thin films revealed persistent ferromagnetism even across a metal–insulator transition. This challenges the current theoretical predictions, and the nature of the local spin state underlying this robustness remains unresolved. Here, we employ high-resolution resonant inelastic x-ray scattering (RIXS) at the Co-L_3 edge to probe the spin states of strained $SrCoO_3$ thin films. Compared with CoO_6 cluster multiplet calculations, we identify a ground state composed of a mixed high- and low-spin configuration, distinct from the previously proposed intermediate-spin state. Our results demonstrate that the robustness of ferromagnetism arises from the interplay between this mixed spin state and the presence of ligand holes associated with negative charge transfer. Our results establish a nontrivial magnetic ground state and offer new pathways for designing robust ferromagnetic phases in correlated oxides.

Keywords: mixed spin states, resonant inelastic x-ray scattering, multiplet ligand-field theory

PACS: 75.30.Wx, 78.70.Ck, 71.27.+a

DOI: 10.1088/1674-1056/ae881c **CSTR:** 32038.14.CPB.ae881c

Transition-metal oxides display a wide variety of emergent phenomena due to the delicate interplay between spin, charge, orbital, and lattice degrees of freedom. A central challenge in this field is the determination of the spin-state configuration, which directly governs the electronic structure and emergent properties. In strongly correlated systems, competing spin states can be nearly degenerate due to the interplay of crystal-field splitting, Hund's coupling, and covalency, making their experimental identification highly nontrivial. Determining spin-state configurations has broad implications across transition-metal oxides, where spin-state transitions are closely linked to emergent phenomena such as superconductivity and Mott transitions.[1–4] Cobalt oxides are particularly challenging in this regard due to their strong covalency and sensitivity to temperature, doping, and strain.[5–8] Among them, $SrCoO_3$, a ferromagnetic metal with promising applications in energy technologies,[9–11] has attracted considerable attention as it has been proposed to host an unusual intermediate-spin state ($S = 3/2$) with a $d^6\underline{L}$ configuration.[12] Its ferromagnetic metallic ground state is highly sensitive to oxygen vacancies, doping, and lattice strain. Density functional theory (DFT) calculations predict a transition from the metallic ferromagnetic (FM) state to an antiferromagnetic (AFM) metallic state at 2% tensile strain.[13] Experimentally, such a transition has indeed been observed in oxygen-deficient $SrCoO_{3-\delta}$ ($\delta < 0.2$) thin films under tensile strain.[14] However, isolating the pure effect of strain is challenging because tensile strain often induces oxygen vacancies in the unstable stoichiometric $SrCoO_3$ phase.[15]

Recent advances in epitaxial growth and post-deposition ozone annealing techniques have enabled the synthesis of stoichiometric $SrCoO_3$ thin films under controlled strain.[16] Intriguingly, these films exhibit a metal–insulator transition (MIT) under 2% tensile strain, while retaining robust ferromagnetism below a Curie temperature (T_C) of 250 K even under strains up to 3%, as confirmed by x-ray magnetic circular dichroism (XMCD) measurements.[16] This strain-insensitive magnetism contrasts sharply with theoretical predictions,[13]

†Corresponding author. E-mail: yilu@nju.edu.cn
‡Corresponding author. E-mail: yingying.peng@pku.edu.cn

© 2026 Chinese Physical Society and IOP Publishing Ltd. All rights, including for text and data mining, AI training, and similar technologies, are reserved.

CPB Online-In-Press

suggesting a non-trivial interplay between electronic correlations and spin states. Resolving the local spin configuration is therefore essential to uncover the microscopic origin of robust ferromagnetism in $SrCoO_3$. More recent dynamical mean-field theory (DMFT) calculations point to a complex admixture of spin and charge states involving fluctuating Co 3d occupations.[17] These contrasting models underscore the need for direct experimental evidence to establish the true spin-state character of $SrCoO_3$.

In this work, we employ high-resolution Co-L_3 edge resonant inelastic x-ray scattering (RIXS) at beamline ID32 of ESRF[18] to directly probe the spin states of $SrCoO_3$ thin films ($\sim$ 30 nm) under varying tensile strains (1%–3%). By tracking the evolution of local dd excitations across the T_C, we observe a pronounced temperature-dependent change in spectral intensity, which cannot be attributed to magnetic or phonon excitations. Through detailed comparison with multiplet calculations, we identify the ground state as a mixture of high-spin and low-spin configurations, in contrast to the previously proposed intermediate-spin state.[12] Importantly, this mixed-spin state is stabilized by strong hybridization with ligand orbitals in a negative charge-transfer regime. The local spin-state excitations remain nearly unchanged from 1% to 3% tensile strain, even as strain drives a metal–insulator transition, demonstrating a pronounced decoupling between the local magnetic configuration and itinerant charge transport. Our results provide direct spectroscopic evidence linking mixed spin states and negative charge transfer to the stabilization of unconventional ferromagnetism in correlated cobalt oxides.

In order to investigate the nature of the excitations in $SrCoO_3$ thin films, we performed RIXS measurements across the Co L_3 edge in 0.25 eV steps for $SrCoO_3/La_{0.3}Sr_{0.7}Al_{0.65}Ta_{0.35}O_3$ (SCO_3/LSAT) at 25 K and 270 K [Figs. 1(a) and 1(b)]. The temperature of 270 K ($\sim$ 20 K above T_C) ensures a paramagnetic state while minimizing sample degradation under x-ray irradiation. The total energy resolution was $\sim$ 50 meV; additional experimental details are provided in Ref. [19]. Several Raman-like features are observed, characterized by energy-loss peaks that remain constant with varying incident photon energy. To quantitatively analyze these features, we fitted the RIXS spectra using Gaussian profiles and identified four distinct excitations. At 25 K, peaks are observed at approximately 0.06 eV, 0.32 eV, 0.70 eV, and 0.98 eV [Fig. 1(c)]; at 270 K, they shift slightly to 0.06 eV, 0.36 eV, 0.73 eV, and 0.93 eV [Fig. 1(d)]. The higher-energy excitations between 0.3 and 1.0 eV are consistent with local dd crystal field transitions,[20,21] whose energies exceed those of phonons ($<$ 90 meV) and magnetic excitations ($\leq$ 50 meV) typically observed in cobalt oxides.[22–27]

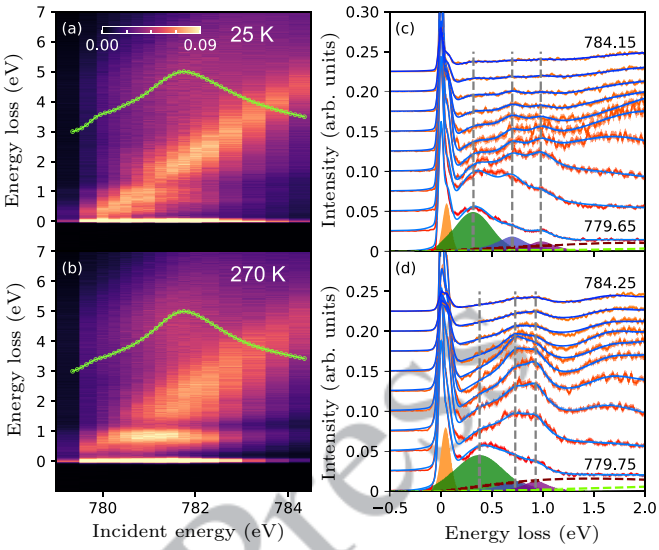


Fig. 1. RIXS spectra of SCO_3/LAST thin films at $\boldsymbol{q} = (0.2, 0.2, 0.2)$ using π-polarized incident x-rays. (a), (b) RIXS intensity map versus energy loss and detuning energy across the Co L_3-edge at 25 K and 270 K, respectively. Intensity is shown on a linear color scale. The green lines are Co L_3-edge x-ray absorption spectra with π-polarized incident x-rays collected at 25 K and 270 K, respectively, measured via total electron yield (TEY). (c), (d) Selected RIXS spectra of incident-energy detuning measurements at 25 K and 270 K with 0.5 eV incident energy interval, respectively. Each spectrum and fitting component are shifted vertically for clarity. Vertical lines indicate Raman-like features.

To gain further insight into the Raman-like features observed below 0.1 eV, we performed high-resolution RIXS measurements with an overall energy resolution of $\sim$ 28 meV. Momentum-resolved RIXS spectra at the Co L_3-edge resonance (781.7 eV) were collected along the two high-symmetry directions, [101] and [111], as shown in Figs. 2(a) and 2(d), with full experimental details provided in Ref. [19]. To reveal the low-energy excitations, the elastic peaks were subtracted from the spectra. The fits of the RIXS spectra are shown in Figs. 2(e) and 2(f) and also in the supplemental material.[19] Two distinct excitations are identified at energies of $\sim$45 meV and 80 meV. These features exhibit negligible momentum and temperature dependence along both measured directions, indicating their local origin. Their intensities increase by approximately 20%–70% at 270 K relative to 25 K.[19] This behavior is not typical of conventional dispersive magnetic excitations reported in related cobalt oxides,[26,28,29] although a magnetic contribution cannot be excluded solely from the absence of measurable dispersion, particularly in the presence of strong damping. Likewise, the strongly asymmetric intensity enhancement with temperature observed here is incompatible with phonon excitations, for which thermal population would increase both Stokes and anti-Stokes signals according to detailed balance, as reflected by the slight enhancement of the anti-Stokes peak in Fig. 2(f). Structural transitions are also excluded based on our x-ray diffraction measurements.[19] Taken together with the multiplet calculations discussed below, these observations support an assignment of the low-energy features to local electronic excitations associated with the tempera-

CPB Online First

ture evolution of the mixed-spin ground state, while possible magnetic or phononic contributions cannot be completely excluded.

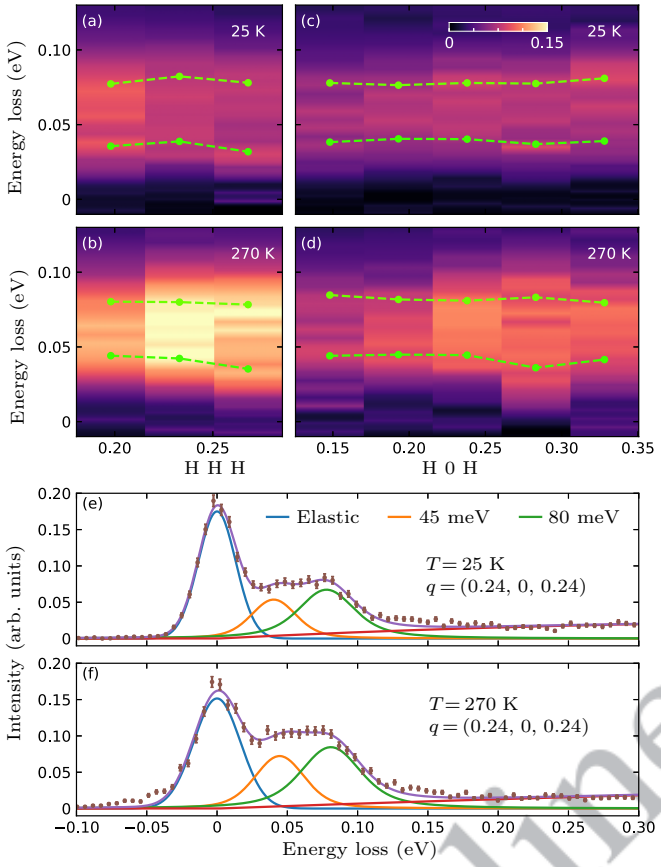


Fig. 2. (a)–(d) Momentum dependence of low-energy features along [111] and [101] directions for SCO_3/LAST thin films at 25 K and 270 K. Intensities are normalized to the 1.5–2.5 eV range and displayed on a linear color scale. The elastic peaks are subtracted. The fit energies of two peaks are overlaid to the intensity map as green markers. (e), (f) The representative spectra and their fitting at momentum-transfer $\boldsymbol{q} = (0.24, 0, 0.24)$ at 25 K and 270 K, respectively.

To investigate the effect of epitaxial strain, we measured the $SrCoO_3$ thin films grown on LSAT, $SrTiO_3$ (STO), and $DyScO_3$ (DSO) substrates, which impose tensile strains of approximately 1%, 2%, and 3%, respectively. For comparison, we also examined an as-grown $SrCoO_{2.5}$ ($SCO_{2.5}$) thin film. The growth procedures and structural characterization of all films are detailed in Ref. [16]. Figure 3 presents the RIXS spectra for these samples measured at 25 K and 270 K. In the $SCO_{2.5}$ film, the low-energy excitations change only slightly with temperature. In contrast, all SCO_3 films exhibit a pronounced increase by more than 50% in the intensity of low-energy excitations at 270 K relative to 25 K, while the excitation energies remain essentially constant across all strain levels. The high-energy dd excitations also show negligible variation with strain.[19] These results demonstrate that tensile strain does not substantially alter the local mixed-spin configuration, despite driving a pronounced evolution of the electronic transport and a metal–insulator transition. Strain therefore primarily modifies the itinerant electronic sector, while the local spin state and ferromagnetic order remain largely intact. This decoupling indicates that the robust ferromagnetism is not governed by itinerant carriers, but is instead supported by the mixed-spin configuration and ligand-hole-mediated exchange. Although $SCO_{2.5}$ crystallizes in a distinct structure, its high Néel temperature ($\sim$ 570 K) precludes any magnetic transition in the measured temperature range, making it an effective reference to distinguish intrinsic changes associated with the ferromagnetic transition in $SrCoO_3$ from thermal effects.

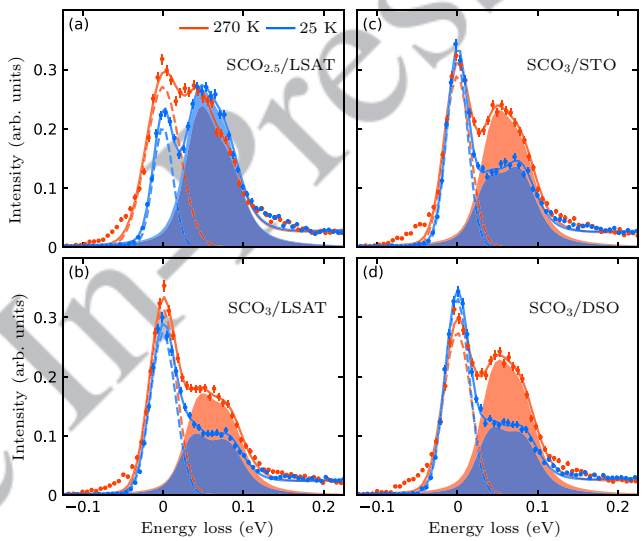


Fig. 3. RIXS spectra measured at the Co L_3-edge resonance (781.7 eV) at 25 K and 270 K for (a) $SCO_{2.5}$/LSAT (reference), (b) SCO_3/LSAT, (c) SCO_3/STO, and (d) SCO_3/DSO with tensile strains of 1%, 2%, and 3%, respectively. The momentum transfer is $\boldsymbol{q} = (0.2, 0.2, 0.2)$. The elastic and low-energy excitations are marked with the dashed line and shaded areas.

To interpret our experimental results, we performed multiplet calculations on a CoO_6 cluster within the framework of ligand field theory,[30] as detailed in the supplemental material.[19] Assuming a nominal Co^{4+} valence state, the cluster contains 15 electrons distributed over 20 spin-orbitals, allowing for three possible total spin configurations: high-spin (HS, $S = 5/2$), intermediate-spin (IS, $S = 3/2$), and low-spin (LS, $S = 1/2$). In modeling $SrCoO_3$, we adopted a negative charge transfer energy, in contrast to the positive charge transfer energy used for $SrCoO_{2.5}$ [Fig. 4(a)]. By tuning the crystal field splitting parameter $10Dq$ from 0.6 eV to 1.1 eV, we constructed the energy-level diagram shown in Fig. 4(b). This diagram indicates that the ground state favors either HS or LS character, depending on the interplay between crystal field strength and Hund's coupling.[31,32] When spin-orbital coupling (SOC) is included in the Co 3d shell, a crossover regime emerges in which the ground state exhibits a mixed HS–LS character. Our calculated phase diagram differs from previous work reporting a stable IS state over a range of crystal field values,[12] primarily due to stronger CoO hybridization in our model. Specifically, we used $V_{e_g} = 3.25$ eV and

CPB Online In-press

$V_{t_{2g}} = 1.8$ eV, almost 67% higher than the values reported in Ref. [12]. These hybridization strengths are supported by independent DFT studies[33,34] and are consistent with values found in other cobaltates featuring a similar CoO_6 cluster geometry.[35]

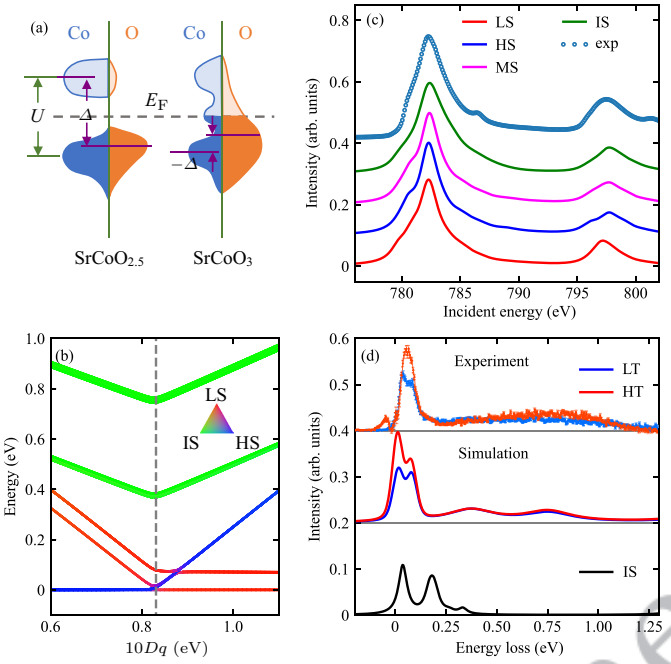


Fig. 4. (a) Illustration of energy band of positive charge-transfer (CT) energy material $SrCoO_{2.5}$ and negative CT energy material $SrCoO_3$. The CT energy is defined as the difference between the total energy with one ligand hole and with a full occupied ligand. As there are average 0.5 and 1 holes in ligand orbitals, the reference level is chosen at Fermi level and lower Hubbard band. (b) Calculated energy diagram of a CoO_6 cluster. The gray line indicates the crystal field energy used in the calculation. The color of energy levels corresponds with the distribution of total spin, as shown in the triangle. (c) Comparison of Co L-edge XAS spectrum collected in total electron yield (TEY) mode and σ polarization to the calculated XAS with different spin states. (d) Experimental RIXS spectra (top), simulated spectra using the crystal-field parameters indicated by the dashed line in panel (b) (middle) at 270 K (HT) and 25 K (LT), and simulated spectra assuming an intermediate-spin (IS) configuration (bottom). All spectra are shown after subtraction of the elastic contribution.

Figure 4(c) shows the calculated XAS spectra for HS, LS, IS, and mixed HS–LS (MS) states, alongside the experimental data. The Co L_3 edge features a main peak with a lower-energy shoulder, and the L_2 edge displays a broad single peak. Although prior work suggested good agreement with the IS state,[12] the subtle spectral differences make it difficult to reach a definitive conclusion based on XAS alone. To resolve this, we computed the RIXS spectra, shown in Fig.4(d), using the crystal field parameter indicated by the dashed line in Fig.4(b). The red and blue curves correspond to low and high temperatures, respectively, with identical parameters except for a small exchange field applied at low temperature to simulate ferromagnetic spin alignment. Both spectra show similar excitation energies but differing intensities. The pronounced enhancement below 0.1 eV arises from the transitions between LS states split by SOC, matching the experimental low-energy feature. Our calculations on RIXS spectra reveal significant intensity for the spin-flip processes including from LS to IS and HS to IS states due to the strong SOC on the Co 2p core shell but negligible RIXS intensity for HS to LS excitations.[19] For comparison, the calculated spectrum for an IS ground state using the parameters of Ref. [12] exhibits pronounced peaks near 0.2 eV and 0.3 eV but little spectral weight between 0.4 eV and 1.0 eV, in clear disagreement with the experimental line shape. Moreover, a purely IS ground state cannot account for the observed temperature dependence of the d–d excitations. Although the comparison does not exclude every possible IS admixture, it strongly disfavors an IS-dominated ground state within the physically relevant parameter regime and instead supports a mixed HS–LS configuration in $SrCoO_3$.

Previous DMFT calculations[17] identified a distribution of spin states on Co 3d orbitals in $SrCoO_3$, with the d^6 high-spin (HS, $S = 2$) configuration dominating at approximately 40%, followed by the intermediate-spin (IS, $S = 1$) state at approximately 20%. Our cluster calculations, which consider the total spin of the full CoO_6 cluster, including the contributions of the ligands, provide an extended perspective. We find a broad distribution of charge states, with d^5, d^6, d^7, and d^8 configurations occurring with probabilities of 22%, 52%, 23%, and 2%, respectively. Within the dominant d^6 component, the total-spin probabilities are 33% for $S = 2$, 15% for $S = 1$, and 4% for $S = 0$. These results are consistent with the DMFT trends but underscore the critical role of ligand hybridization and spin–charge entanglement in stabilizing the mixed-spin ground state.

The metal–insulator transition in $SrCoO_3$ occurs without any accompanying magnetic phase transition, highlighting the unusual decoupling between charge and spin degrees of freedom in this system. In contrast, the related positive charge transfer compound $SrCoO_{2.5}$ exhibits robust G-type AFM order up to 570 K.[36] Similarly, in iron oxides, the positive charge transfer compound $Sr_2Fe_2O_5$ exhibits AFM order up to $\sim$ 690 K.[37] These results suggest a critical role for charge transfer energy in determining the magnetic ground state and its stability. To elucidate the origin of magnetic coupling in $SrCoO_3$, we constructed a model including 3d orbitals of two cobalt sites and their corresponding ligand orbitals, allowing us to compute the ground state evolution as a function of charge transfer energy.[38] Following the same approach as in our single-site analysis, the model includes twenty Co 3d orbitals and twenty ligand orbitals, formed from linear combinations of the 2p orbitals of eleven surrounding oxygen atoms that directly hybridize with Co. We computed the 48 lowest-energy eigenstates (Fig. 5) and analyzed both the local spin distribution on a single Co site and the total spin of the entire cluster to determine the spin state and magnetic exchange

CPB Online In Press

interaction. For charge-transfer energy $\Delta > 0.8$ eV, the Co ions adopt high-spin configurations, yet the total cluster spin remains small, indicating antiferromagnetic (AFM) coupling. In the intermediate regime -1.6 eV $\leq \Delta \leq 0.8$ eV, the total spin increases, signifying ferromagnetic (FM) coupling. Notably, in the range -1.6 eV $\leq \Delta \leq -1.0$ eV, the Co ions exhibit mixed spin states. At more negative values of Δ, the Co ions transition into low-spin states, and the system becomes paramagnetic. These results are compared with the single-site cluster model (inset of Fig. 5(b)), which shows a narrow mixed-spin regime (< 0.1 eV), in contrast to the much broader range (~ 0.6 eV) observed in the two-site cluster. These results demonstrate the intrinsic stability of mixed-spin configurations in $SrCoO_3$ and underscore the important role of negative charge-transfer energy and persistent ligand holes in mediating ferromagnetic interactions. Such ligand-hole-stabilized spin states and ferromagnetic couplings shed light on the complex behavior of related systems, including the unusual layer order in high-valence double-perovskite iron oxides,[39] the strongly frustrated nearest-neighbor superexchange in perovskite nickelates,[40,41] and the anomalously weak intralayer magnetic interactions in the bilayer nickelate superconductor,[42] which may play an important role in determining the pairing symmetry.[43]

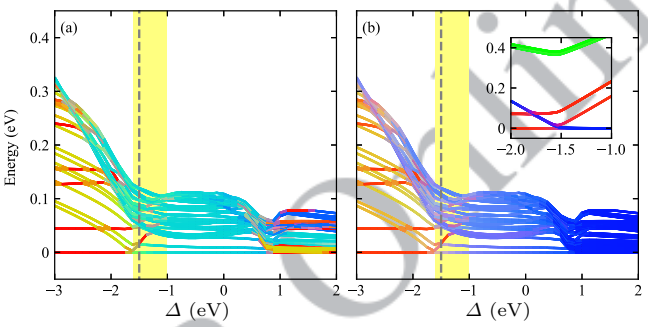


Fig. 5. The energy diagram for a double-site cluster of $SrCoO_3$. (a) The color assigned to each energy level denotes the total spin of the entire cluster. Specifically, red, green, and blue colors correspond to approximate total spin values of 0.5, 2, and 3.5, respectively. (b) The spin state on one Co atom as Fig. 4(b) in the main text. The yellow shaded area indicates the range of mixed spin state and the dashed line indicates the charge transfer energy in XAS and RIXS spectra calculation. The inset shows the energy diagram of the one site ligand field model.

Our RIXS measurements show that the local electronic structure in $SrCoO_3$ thin films remains largely insensitive to epitaxial strain, consistent with previous XAS and XMCD studies.[16] Our calculations yield a local magnetic moment of the CoO_6 cluster of approximately 2.8 μ_B in the low-temperature limit, in good agreement with the experimentally reported saturation moment of ~ 2.5 μ_B from magnetization measurements.[44] In the negative charge-transfer regime, the nominal Co^{4+} state has substantial $d^6\underline{L}$ character, with holes residing predominantly in strongly hybridized O 2p–Co 3d states. Hopping of these ligand holes between neighboring CoO_6 units lowers the kinetic energy when the Co moments are aligned, producing an oxygen-hole-mediated, double-exchange-like ferromagnetic interaction. Unlike conventional mixed-valence double exchange between distinct Co^{3+} and Co^{4+} sites, the relevant carriers here are ligand holes. Their persistence under tensile strain allows the ferromagnetic alignment to survive even when coherent charge transport is strongly suppressed. Although the mixed-spin state is relatively unaffected by strain, alternative tuning parameters, such as chemical doping or electrostatic gating, can shift the high-spin–low-spin balance (HS–LS) and stabilize emergent magnetic phases. For example, ionic liquid gating enables a reversible transformation between $SrCoO_{2.5}$ and $SrCoO_3$ by modulating oxygen vacancies.[45,46] On the other hand, substituting Sr with La dopes electrons and stabilizes the low-spin ($S = 0$) ground state at low temperatures.[20,47] The combined control of oxygen stoichiometry and carrier density therefore provides a powerful route to engineer magnetic ground states, as demonstrated in recent studies.[48]

In summary, by combining high-resolution RIXS measurements with multiplet cluster calculations, we identify the ground state of strained $SrCoO_3$ thin films as a mixture of high-spin and low-spin configurations. This mixed-spin ground state, stabilized by strong Co–O hybridization and negative charge transfer energy, accounts for the persistence of ferromagnetism across the strain-induced metal–insulator transition and rules out the previously proposed intermediate-spin scenario. Strain substantially modifies charge transport but has little effect on the local mixed-spin configuration, indicating that the robust ferromagnetism is governed primarily by spin–ligand entanglement and ligand-hole-mediated exchange rather than by strain-induced changes in the local spin state. More broadly, these results highlight the important role of strong p–d hybridization and the additional degrees of freedom provided by persistent ligand holes in stabilizing unconventional ground states in negative-charge-transfer and strongly hybridized materials. This insight points to new strategies for engineering strain-resilient magnetic states by tuning spin–ligand entanglement, for example via electrostatic gating or chemical substitution.

Acknowledgements

Y.Y.P. is grateful for financial support from the National Natural Science Foundation of China (Grant Nos. 12374143 and 11974029), the National Key R&D Program of China (Grant Nos. 2019YFA0308401 and 2021YFA1401903), and Beijing Natural Science Foundation (Grant No. JQ24001). Y.L. acknowledges the financial support from the National Key R&D Program of China (Grant No. 2022YFA1403000) and the National Natural Science Foundation of China (Grant No. 12274207). P.Y. acknowledges the financial support from the National Natural Science Foundation of China (Grant

Chin. Phys. B Online In-Press

Nos. 52025024 and 12421004) and the National Key R&D Program of China (Grant No. 2023YFA1406400). The experimental data were collected at the beam line ID32 of the European Synchrotron Radiation Facility (ESRF) in Grenoble (F) using the ERIXS spectrometer designed jointly by the ESRF and Politecnico di Milano (Proposal No. HC-4813).

References

[1] Chaloupka J C V and Khaliullin G 2025 *Phys. Rev. B* **112** 075157
[2] Oh H, Wu Y M, May-Mann J, Yu Y, Hwang H Y, Zhang Y H and Raghu S 2026 *Phys. Rev. B* **113** 024430
[3] Lyubutin I S, Ovchinnikov S G, Gavriliuk A G and Struzhkin V V 2009 *Phys. Rev. B* **79** 085125
[4] Kunes J, Lukoyanov A V, Anisimov V I, Scalettar R T and Pickett W E 2008 *Nat. Mater.* **7** 198
[5] Hu Z, Wu H, Haverkort M W, Hsieh H H, Lin H J, Lorenz T, Baier J, Reichl A, Bonn I, Felser C, Tanaka A, Chen C T and Tjeng L H 2004 *Phys. Rev. Lett.* **92** 207402
[6] Tian D, Zheng H, Huang Z, Wu S, Li P, Li C, Zhang J, Shu X, Zhou J, Liu Y, Gu Y, Wang M, Yi D, Nan T, Chen Z, He Q, Wu H, Zhou S, Luo W and Yu P 2025 *Phys. Rev. X* **14** 041030
[7] Takegami D, Tanaka A, Agrestini S, Hu Z, Weinen J, Rotter M, Schussler-Langeheine C, Willers T, Koethe T C, Lorenz T, Liao Y F, Tsuei K D, Lin H J, Chen C T and Tjeng L H 2023 *Phys. Rev. X* **13** 011037
[8] Vogt T, Woodward P M, Karen P, Hunter B A, Henning P and Moodenbaugh A R 2000 *Phys. Rev. Lett.* **84** 2969
[9] He Y, Wang Y, Qian J, Xu K, Lu B, Tang S, Liu Y and Shen J 2025 *Appl. Catal. B: Environ. Energy* **361** 124565
[10] Fu L, Li Z, Shang X and Zhang W 2025 *Appl. Catal. B: Environ. Energy* **379** 125732
[11] He J, Zhou Y, Wu S, Jin L, Cao J, Demir M and Ma P 2024 *Inorg. Chem.* **63** 13755
[12] Potze R H, Sawatzky G A and Abbate M 1995 *Phys. Rev. B* **51** 11501
[13] Lee J H and Rabe K M 2011 *Phys. Rev. Lett.* **107** 067601
[14] Callori S J, Hu S, Bertinshaw J, Yue Z J, Danilkin S, Wang X L, Nagarajan V, Klose F, Seidel J and Ulrich C 2015 *Phys. Rev. B* **91** 140405
[15] Petrie J R, Mitra C, Jeen H, Choi W S, Meyer T L, Reboredo F A, Freeland J W, Eres G and Lee H N 2016 *Adv. Funct. Mater.* **26** 1564
[16] Wang Y, He Q, Ming W, Du M H, Lu N, Cafolla C, Fujioka J, Zhang Q, Zhang D, Shen S, Lyu Y, N'Diaye A T, Arenholz E, Gu L, Nan C, Tokura Y, Okamoto S and Yu P 2020 *Phys. Rev. X* **10** 021030
[17] Kunes J, Krapek V, Parragh N, Sangiovanni G, Toschi A and Kozhevnikov A V 2012 *Phys. Rev. Lett.* **109** 117206
[18] Brookes N B, Yakhou-Harris F, Kummer K, Fondacaro A, Cezar J, Betto D, Velez-Fort E, Amorese A, Ghiringhelli G, Braicovich L, Barrett R, Berruyer G, Cianciosi F, Eybert L, Marion P, van der Linden P and Zhang L 2018 *Nucl. Instrum. Methods Phys. Res. A* **903** 175
[19] See supplemental material for more details
[20] Tomiyasu K, Okamoto J, Huang H Y, Chen Z Y, Sinaga E P, Wu W B, Chu Y Y, Singh A, Wang R P, de Groot F M F, Chainani A, Ishihara S, Chen C T and Huang D J 2017 *Phys. Rev. Lett.* **119** 196402
[21] Wang R P, Hariki A, Sotnikov A, Frati F, Okamoto J, Huang H Y, Singh A, Huang D J, Tomiyasu K, Du C H and Kunes J 2018 *Phys. Rev. B* **98** 035149
[22] Yuan B, Khait I, Shu G J, Chou F C, Stone M B, Clancy J P, Paramekanti A and Kim Y J 2020 *Phys. Rev. X* **10** 011062
[23] Elliot M, McClarty P A, Prabhakaran D, Johnson R D, Walker H C, Manuel P and Coldea R 2021 *Nat. Commun.* **12** 3936
[24] Mitra C, Fishman R S, Okamoto S, Lee H N and Reboredo F A 2013 *J. Phys.: Condens. Matter* **26** 036004
[25] Jost D, Lomeli E G, Kim W J, Been E M, Rossi M, Agrestini S, Zhou K J, Jia C, Moritz B, Shen Z X, Hwang H Y, Devereaux T P and Lee W S 2025 *npj Quantum Mater.* **10** 60
[26] Sarte P M, Songvilay M, Pachoud E, Ewings R A, Frost C D, Prabhakaran D, Hong K H, Browne A J, Yamani Z, Attfield J P, Rodriguez E E, Wilson S D and Stock C 2019 *Phys. Rev. B* **100** 075143
[27] Orlovskaya N, Steinmetz D, Yarmolenko S, Pai D, Sankar J and Goodenough J 2005 *Phys. Rev. B* **72** 014122
[28] Ewings R A, Freeman P G, Enderle M, Kulda J, Prabhakaran D and Boothroyd A T 2010 *Phys. Rev. B* **82** 144401
[29] Shamoto S, Yamauchi H, Ikeuchi K, Kajimoto R and Ieda J 2021 *Phys. Rev. Research* **3** 013169
[30] Haverkort M W, Zwierzycki M and Andersen O K 2012 *Phys. Rev. B* **85** 165113
[31] Zobel C, Kriener M, Bruns D, Baier J, Gruninger M, Lorenz T, Reutler P and Revcolevschi A 2002 *Phys. Rev. B* **66** 020402
[32] Kumar V, Kumar R, Shukla D, Arora S, Shvets I, Singh K and Kumar R 2014 *Mater. Chem. Phys.* **147** 617
[33] Cardot C A, Kas J J, Abramson J E, Rehr J J and Seidler G T 2024 *J. Electron Spectrosc. Relat. Phenom.* **270** 147419
[34] Gorelov E, Guda A, Soldatov M, Guda S, Pashkov D, Tanaka A, Lafuerza S, Lamberti C and Soldatov A 2020 *Radiat. Phys. Chem.* **175** 108105
[35] Wang R P, Huang M J, Hariki A, Okamoto J, Huang H Y, Singh A, Huang D J, Nagel P, Schuppler S, Haarman T, Liu B and de Groot F M F 2022 *J. Phys. Chem. C* **126** 8752
[36] Munoz A, de la Calle C, Alonso J A, Botta P M, Pardo V, Baldomir D and Rivas J 2008 *Phys. Rev. B* **78** 054404
[37] Schmidt M and Campbell S 2001 *J. Solid State Chem.* **156** 292
[38] Green R J, Haverkort M W and Sawatzky G A 2016 *Phys. Rev. B* **94** 195127
[39] Yang K, Khomskii D I and Wu H 2018 *Phys. Rev. B* **98** 085105
[40] Piamonteze C, de Groot F M F, Tolentino H C N, Ramos A Y, Massa N E, Alonso J A and Martinez-Lope M J 2005 *Phys. Rev. B* **71** 020406
[41] Lu Y, Betto D, Fursich K, Suzuki H, Kim H H, Cristiani G, Logvenov G, Brookes N B, Benckiser E, Haverkort M W, Khaliullin G, Le Tacon M, Minola M and Keimer B 2018 *Phys. Rev. X* **8** 031014
[42] Chen X, Choi J, Jiang Z, Mei J, Jiang K, Li J, Agrestini S, Garcia-Fernandez M, Sun H, Huang X, Shen D, Wang M, Hu J, Lu Y, Zhou K J and Feng D 2024 *Nat. Commun.* **15** 9597
[43] Lu C, Pan Z, Yang F and Wu C 2024 *Phys. Rev. Lett.* **132** 146002
[44] Long Y, Kaneko Y, Ishiwata S, Taguchi Y and Tokura Y 2011 *J. Phys.: Condens. Matter* **23** 245601
[45] Lu N, Zhang P, Zhang Q, Qiao R, He Q, Li H B, Wang Y, Guo J, Zhang D, Duan Z, Li Z, Wang M, Yang S, Yan M, Arenholz E, Zhou S, Yang W, Gu L, Nan C W, Wu J, Tokura Y and Yu P 2017 *Nature* **546** 124
[46] Cui B, Werner P, Ma T, Zhong X, Wang Z, Taylor J M, Zhuang Y and Parkin S S P 2018 *Nat. Commun.* **9** 3055
[47] Klie R F, Zheng J C, Zhu Y, Varela M, Wu J and Leighton C 2007 *Phys. Rev. Lett.* **99** 047203
[48] Biskup N, Salafranca J, Mehta V, Oxley M P, Suzuki Y, Pennycook S J, Pantelides S T and Varela M 2014 *Phys. Rev. Lett.* **112** 087202

Chinese Physics B Press